Damping of $Co_xFe_{80-x}B_{20}$ ultrathin films with perpendicular magnetic anisotropy

T. Devolder,[1,2,a)] P.-H. Ducrot,[1,2] J.-P. Adam,[1,2] I. Barisic,[1,2] N. Vernier,[1,2] Joo-Von Kim,[1,2] B. Ockert,[3] and D. Ravelosona[1,2]
[1]*Institut d'Electronique Fondamentale, CNRS, UMR 8622, Orsay, France*
[2]*Univ. Paris-Sud, 91405 Orsay, France*
[3]*Singulus Technology AG, Hanauer Landstrasse 103, 63796 Kahl am Main, Germany*

(Received 26 November 2012; accepted 26 December 2012; published online 15 January 2013)

We use vector network analyzer ferromagnetic resonance to study the perpendicularly magnetized CoFeB films. We report the dependence of the anisotropy, the g-factor, and the damping upon the Fe-Co compositional ratio in the amorphous and crystalline states. The damping and the anisotropy increase upon crystallization but vary little with composition on the Fe-rich side. At high cobalt content, the anisotropy lowers while the damping and the sample inhomogeneity increase. The compositional dependences seem to extrapolate from the properties of bulk CoFe alloys, with differences that can be understood from the correlated impacts of spin-orbit interaction on anisotropy, g-factor, and damping. © *2013 American Institute of Physics*. [http://dx.doi.org/10.1063/1.4775684]

The seminal work of Ikeda *et al.*[1] showed that magnetic tunnel junctions with ultrathin CoFeB free layers could exhibit both a perpendicular magnetic anisotropy (PMA) and a reasonably low damping, making them a promising candidate for the next generation of magnetic random access memories. Unfortunately, the damping was reported to increase very substantially at low thicknesses,[2] being for instance[1] already 0.027 at 1.3 nm, which is detrimental to the use of thinner layers in spin-torque operated devices. Understanding the damping parameters of CoFeB alloys with PMA is thus crucial to minimize it and to assess the technological potential of this class of alloys. While their quasi-static magnetic properties are known,[3,4] there is a lot of scatter in the reported dynamic properties[5,6] of CoFeB alloys, and little is known about the compositional dependence of these properties. In particular, the reports of damping measurements were so far mainly done by time-domain methods like time-resolved magneto-optical Kerr effect[6,7] which have a limited precision and are not free of artifacts. Unfortunately, the ferromagnetic resonance methods previous applied on in-plane magnetized thick CoFeB layers[2,8] were so far not sensitive enough[6] to characterize the strongly anisotropic and weakly resonant ultrathin CoFeB layers when having perpendicular magnetization.

In this work, we study ultrathin CoFeB layers with growth conditions optimized for perpendicular magnetic anisotropy. By using vector network analyzer ferromagnetic resonance (VNA-FMR[8]), we measure the compositional dependence and the dependence on thermal treatment of the anisotropy, the gyromagnetic ratio, the Gilbert damping factor α, and the inhomogeneity of the magnetic properties of CoFeB thin films with perpendicular anisotropy. The results can be understood from the parameters known for single crystalline bulk Co_xFe_{1-x} alloys, and from the correlations among the Landé factor, the magneto-crystalline anisotropy, and the Gilbert damping that all scale with the spin-orbit coupling.

Our samples are CoFeB layers of compositions $Co_{20}Fe_{60}B_{20}$, $Co_{40}Fe_{40}B_{20}$ and $Co_{60}Fe_{20}B_{20}$ and thickness $t = 1$ nm. They were grown in a Singulus Timaris deposition machine by dc sputtering on oxidized silicon, on top of a 3 nm Ta buffer. They are caped with 2 nm of MgO and 5 nm of Ta. We studied them in the amorphous as-grown state and after a crystallization induced[4,9] by a 300 °C, 2 h long annealing. The quasi-static magnetic properties of the films were studied and verified using alternative gradient field magnetometry and polar magnetooptical Kerr effect (MOKE) magnetometry.

The high-frequency (0.1 to 70 GHz) characterizations were performed using a VNA-FMR[8] set-up in the open-circuit total reflection configuration.[10] The dc field of 0-2.4 T is applied perpendicular to the sample surface. When it saturates the magnetization, this field orientation prevents[11] any contribution from two-magnon scattering, such that the ferromagnetic resonance linewidth is only influenced by Gilbert damping and long-range inhomogeneities of the internal field (so-called inhomogeneous broadening). Noteworthy, domain wall mobility measurements indicated an exceptionally good uniformity, such that the FMR linewidth is expected to be close to the Gilbert linewidth. Another advantage of this geometry is that it can separate unambiguously the contributions of the Landé factor and the effective magnetization to the ferromagnetic resonance frequency.

In VNAFMR, the sample is placed in the near field of a microwave coplanar waveguide, and the sample magnons exchange energy with the microwave photons. As a result, the frequency dependence of the impedance of this ensemble can be used to extract[8] a quantity proportional to the microwave transverse susceptibility χ_t of the sample. Note that in contrast to conventional FMR methods[2] that only provide the imaginary part (i.e., in-quadrature component) of the susceptibility, our method also provides the real part (i.e., in-phase component) of the susceptibility. The obtained susceptibility is reduced by a filling factor $t/w \approx 10^{-6}$, where w is an effective extension of the RF field, related to the waveguide width and the electromagnetic absorption of the sample, including the substrate conductivity contributions. This factor is constant for our six samples, and it is corrected for in Fig. 2.

a)Electronic mail: thibaut.devolder@u-psud.fr.

To deduce the susceptibility, we need in principle a reference spectrum with vanishing magnetic susceptibility.[10] This cannot be obtained in our geometry, where the RF field orientation is fixed and transverse to the applied field. In practice, we construct a satisfactory estimate of this reference spectrum by averaging spectra over a field window of $\pm$ 120 mT about the resonance. This procedure has the drawback not to be able to provide the susceptibility levels far from the resonance condition, in particular in the dc limit.

To analyze the microwave susceptibility data, we start from an energy density that includes the Zeeman interaction, the shape anisotropy of a film, and a PMA energy written as $E = \frac{1}{2}\mu_0 H_{k1} M_S \sin^2\theta + \frac{1}{4}\mu_0 H_{k2} M_S \sin^4\theta$ with θ the angle between the magnetization and the sample normal. Our convention is that the first and second order magneto-crystalline anisotropy fields $H_{k1} = 2K_1/(\mu_0 M_S)$ and $H_{k2} = 4K_2/(\mu_0 M_S)$ are positive when they favor perpendicular magnetization, i.e., $\theta = 0$. The linearization of the Landau–Lifshitz–Gilbert equation about $\theta = 0$ yields the susceptibility tensor with two equal transverse terms χ_t. The real part of the transverse susceptibility can be written as

$$\Re(\chi_t) = \frac{\gamma_0^2 M_s \tilde{H}(\gamma_0^2 \tilde{H}^2 - \omega^2)}{4\alpha^2\gamma_0^2\tilde{H}^2\omega^2 + (\gamma_0^2\tilde{H}^2 - \omega^2)^2}, \quad (1)$$

where γ_0 is the gyromagnetic ratio and $\tilde{H} = (H - M_S + H_{k1})$ is the stiffness field. Note that in our geometry, the stiffness field does not depend on the second anisotropy field. The real part of the susceptibility reduces to $\chi_{t,dc} = M_S/\tilde{H}$ at $\omega = 0$. The in-phase susceptibility vanishes at the ferromagnetic resonance frequency $\omega_{FMR}/(2\pi)$ with $\omega_{FMR} = \gamma_0\tilde{H}$. Linear fits of the ω_{FMR} versus H curves are used to get γ_0, which is then translated in a spectroscopic splitting factor g. The zero-field intercept of the curve is then used to derive the effective anisotropy field $H_{k1} - M_S$.

The imaginary part of the transverse susceptibility is

$$\Im(\chi_t) = \frac{\alpha\gamma_0 M_s \omega(\gamma_0^2\tilde{H}^2 + \omega^2)}{4\alpha^2\gamma_0^2\tilde{H}^2\omega^2 + (\gamma_0^2\tilde{H}^2 - \omega^2)^2}. \quad (2)$$

It is peaked at the FMR frequency, with a peak amplitude of $\frac{\chi_{dc}}{2\alpha}$ and a peak area of $\approx \gamma_0 M_S$, independent from the damping parameter. The positive peak to negative peak frequency spacing of $\Re(\chi_t)$ or equivalently the full width at half maximum of the peak of $\Im(\chi_t)$ is $\Delta\omega = 2\alpha\gamma_0\tilde{H}$. In principle, the algebra $\Delta\omega/(2\omega_{FMR})$ gives the damping parameter, but with our modest signal to noise ratio and the weakly resonating character of PMA samples (see Fig. 2), we generally prefer to fit the entire susceptibility spectrum with Eqs. (1) and (2) to get the linewidth, and then to plot the curve $\Delta\omega/2$ versus ω_{FMR}. The slope of this curve is then the Gilbert damping factor, and the field translation of the zero frequency intercept $\Delta\omega/(2\gamma_0)|_{\omega=0}$ is a measure of the inhomogeneity of the internal field in the sensed area, which is 3 mm $\times$ 200 μm.

Using this model, let us now look at the variation of the magnetic properties of our samples.

Fig. 1 displays the field dependence of the FMR frequencies of ultrathin CoFeB films of variable compositions, either in the crystalline or the amorphous state. These curves

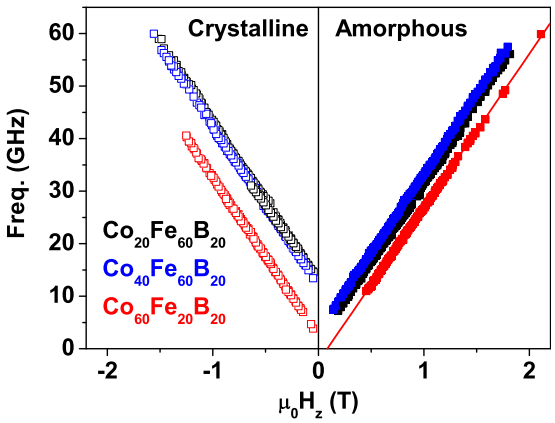

FIG. 1. Field dependence of the ferromagnetic resonance frequencies for various 1 nm thick Ta/CoFeB/MgO layers. The data for the annealed crystalline (as-grown amorphous) samples appear in negative (positive) fields. The line is a fit through $Co_{60}Fe_{20}B_{20}$, in the as-grown (amorphous) state.

are used to extract the anisotropy fields and the g-factors of all samples, as listed in Table I. As already demonstrated earlier for our three compositions,[2,5,9] we confirm a substantial increase of the effective anisotropy upon annealing. This increase of the anisotropy field reorients the easy magnetization axis in the Co-rich samples toward the out-of-plane direction. Before discussing this evolution, let us look at the correlated changes of g and α.

For all samples except the Co-rich sample in the as-grown state, the Landé factor is close to 2.16. The Co-rich sample in the as-grown state has a larger Landé factor. It is interesting to compare our data with bulk, single crystalline Co_xFe_{1-x} alloys, as tabulated in Refs.12 and 13. Indeed boron is a metalloid, such that its orbitals should not significantly alter the band structure of CoFe near the Fermi level. Qualitatively, boron is not expected to have a strong impact on the magnetic properties, apart from the dilution effect of the saturation magnetization.[3] It is known[12,13] that the bulk Co_xFe_{1-x} alloys, which are much more isotropic than our ultra thin films, have a nearly constant g-factor equal to 2.09 for all compositions following $0 \le x \le 0.5$. In bulk CoFe alloys, the g-factor increased to 2.11 for $x = 0.7$, consistent

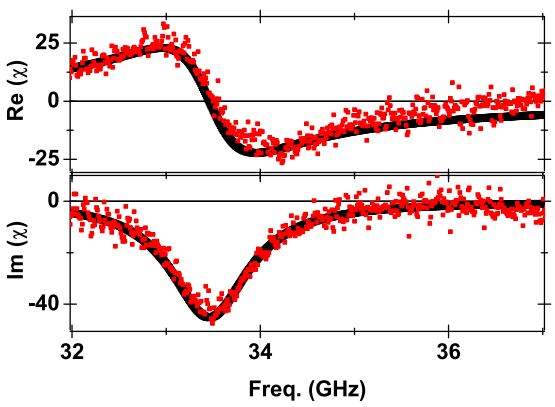

FIG. 2. Example of a permeability spectrum recorded on 1 nm of $Co_{40}Fe_{40}B_{20}$ in the as-grown (amorphous) state for an applied field of 1 T (red dots) perpendicular to the sample. The fit (bold black line) is done using the parameters of Table I, i.e., an "effective" damping $\Delta\omega/(2\omega_{FMR}) = 0015$ at the resonance frequency of 34 GHz. A scaling factor has been applied to the experimental susceptibility level to account for the space filling factor.

TABLE I. Table of the magnetic properties extracted from VNAFMR measurements on 1 nm Ta/CoFeB/MgO films and comparison with relevant literature values."a-" stands for amorphous as-grown state."c-" stands for crystalline annealed state. The error bars apply to the first six raws.

Composition	$\mu_0(H_{k1}-M_S)$ (mT) ± 10	g-factor ± 0.003	α ±0.002	$\Delta\omega/(2\gamma_0)\vert_{\omega=0}$(mT) ± 0.6
a-$Co_{20}Fe_{60}B_{20}$, 1 nm	45	2.159	0.014	6.2
c-$Co_{20}Fe_{60}B_{20}$, 1 nm	430	2.165	0.015	11.1
a-$Co_{40}Fe_{40}B_{20}$, 1 nm	107	2.157	0.012	6.6
c-$Co_{40}Fe_{40}B_{20}$, 1 nm	397	2.161	0.013	8
a-$Co_{60}Fe_{20}B_{20}$, 1 nm	−80	2.186	0.019 ±0.004	11 ± 2
c-$Co_{60}Fe_{20}B_{20}$, 1 nm	82	2.158	0.016	14.5
Bulk c-$Co_{40}Fe_{40}B_{20}$ (Ref. 2)	−1800	2.05–2.09	0.004	
Bulk bcc Fe	−2202	2.088 (Ref. 12), 2.09 (Ref. 13)	0.0019 (Ref. 19)	
Bulk $Co_{25}Fe_{75}$		2.089 (Ref. 12)		
Bulk $Co_{50}Fe_{50}$	−2365 (Ref. 20)	2.092 (Ref. 12) 2.09 (Ref. 13)		
Bulk $Co_{75}Fe_{25}$		2.109 (Ref. 12)		
Bulk $Co_{90}Fe_{10}$		2.160 (Ref. 12)		
Bulk hcp Co (c-axis)	−1160	2.193 (Ref. 12) 2.18 (Ref. 21)	0.008	
Bulk fcc Co (Ref. 15)	−1800	2.16		

with the fact that the g-factor of Co is greater than that of Fe (see Table I), due to a 28% larger spin-orbit coupling.[14] This increase of g at high cobalt content is also seen in our Co-rich ultra thin films in the as-grown state. Note also that the g factor of bulk Co depends on the atomic ordering: it is 2.19 in the bulk hcp state and 2.16 in the more isotropic fcc state.[15] This dependence on the short range order may qualitatively explain why the g-factor of our Co-rich sample decreases substantially when annealing and transforming to a more relaxed[4] and more isotropic (bcc) crystalline state.

An additional striking fact is that our films have Landé factors substantially higher than their bulk counterparts. This could have been anticipated from the large anisotropy fields H_{k1}, since in principle both the magnetocrystalline anisotropy[16] and the increment of the Landé factor are a measure of the orbital momentum μ_L contribution to the magnetization. Indeed the Landé factor follows $\frac{\mu_L}{\mu_S} = g/2 - 1$, where μ_S is the spin momentum, while the anisotropy energy follows the anisotropy of μ_L. This trend is verified semi-quantitatively in our two most iron rich compositions: g and H_{k1} increase together upon annealing (see Table I).

Let us now analyze the damping in our ultra thin films. Fig. 2 displays a representative susceptibility spectrum, taken for the 1 nm $Co_{40}Fe_{40}B_{20}$ film in a field of 1 T. The fit is done using the parameters of Table I. At high frequencies (high applied fields), the linewidths are essentially equal to the Gilbert linewidth, with marginal differences between the two Fe-rich samples that are at the scale of the error bars. At low frequencies, the linewidths are larger than what would be extrapolated from the high frequency data and are significantly larger for the annealed samples. When doing only low field ($H \leq 0.5$ T) experiments, this may give the misleading impression that the damping is much higher in the annealed states. This frequency dependence of the linewidth is indicative of some inhomogeneous linewidth broadening due to a spatial distribution of the internal fields in our ultrathin films, more pronounced in the annealed states.

Once again, it is interesting to compare our data with bulk single crystalline Co_xFe_{1-x} alloys.[13] In bulk alloys, g and the Gilbert linewidth are strongly correlated and are both constant for any composition between $0 \leq x \leq 0.5$. They both increase for $x \geq 0.7$, with a doubling of the damping parameter at this composition. This sheds light on our observation that the damping tends to increase with the cobalt content, especially for $Co_{60}Fe_{20}B_{20}$, i.e., $x = 0.75$. In addition to this sensitivity to the cobalt content, α is also expected to be correlated with the g-factor. Indeed the spin-orbit contribution to the damping parameter[17] yields a dependence following $\alpha \propto (g-2)^2$ in transition metals. We have compiled the $\{g, \alpha\}$ pairs of our present work and from the literature in Fig. 3 to illustrate that this trend is verified qualitatively in CoFeB alloys. The increase of g and H_{k1} upon annealing comes systematically with an increase of α. This consistency between these three parameters strengthens our confidence in the data reported in Table I.

Finally, the zero frequency field linewidth (Table I) indicate a clear increase of sample inhomogeneity upon annealing. This may seem surprising in view of previous works that indicated that the crystallization helps to get a more perfect CoFeB/MgO interface,[9,18] with a correlated increase of the tunnel magneto-resistance.[4] However, even if grazing angle

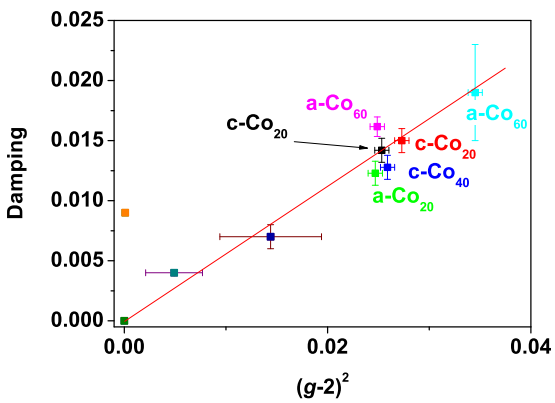

FIG. 3. Gilbert damping parameter versus the square increment of the Landé factor for various $Co_xFe_yB_z$ alloys. Our data are the black symbols. The line is a guide to the eye. The 3 items falling near the line are the $\{0,0\}$ point, then the data from Ref. 2, and Ref. 8 with the g-factor of Ref. 13. The symbol falling away from line is from Ref. 6.

X-ray reflectometry measurements on $Co_{60}Fe_{20}B_{20}$ done by Pym *et al*. have shown that the crystallization comes with a sharpening of the gradient of the chemical composition profile across the CoFeB/MgO interface, the same authors emphasize that this does not improve the topological roughness. It must instead create clearly defined atomic steps between atomically flat terraces. In addition, in the specific case of high Co content, it is also possible that the crystallization is incomplete leaving large bcc grains separated by an matrix that remains amorphous.[4] These two facts must result in a lateral distribution of the surface anisotropy contribution to H_{k1}. In the end, we believe that such an evolution of the material can only reinforce the inhomogenous linewidth broadening, especially at high Co content where the crystallization is less likely to be complete.[4] This linewidth broadening after annealing may explain why previous studies performed on $Co_{20}Fe_{60}B_{20}$ (Ref. 6) concluded in scattered (effective) damping values, with inconsistencies between the high values obtained at low field and the smaller damping obtained and high fields.

In conclusion, we have used VNAFMR to study how the dynamic magnetic properties of CoFeB layers showing PMA depend on the Co-to-Fe compositional ratio and the crystallinity. The spectroscopic splitting factor g, the Gilbert damping α, and the effective anisotropy field $H_{k1} - M_S$ increase with crystallization but are essentially independent of the composition when there is more than 50% of iron. Conversely, at higher cobalt content, the anisotropy lowers while the damping increases, making this composition less interesting for spin-torque based applications. The variations of g, α, and H_{k1} can be understood qualitatively from the properties of bulk CoFe alloys and from the expected impact of spin-orbit interaction on these three quantities.

This work was supported by the European Communities FP7 program through Contract MAGWIRE No. 257707.

[1]S. Ikeda, K. Miura, H. Yamamoto, K. Mizunuma, H. D. Gan, M. Endo, S. Kanai, J. Hayakawa, F. Matsukura, and H. Ohno, Nature Mater. **9**, 721 (2010).
[2]X. Liu, W. Zhang, M. J. Carter, and G. Xiao, J. Appl. Phys. **110**, 033910 (2011).
[3]M. Munakata, S.-I. Aoqui, and M. Yagi, IEEE Trans. Magn. **41**(10), 3262 (2005).
[4]Y. M. Lee, J. Hayakawa, S. Ikeda, F. Matsukura, and H. Ohno, Appl. Phys. Lett. **90**, 212507 (2007).
[5]Y. S. Chen, C.-W. Cheng, G. Chern, W. F. Wu, and J. G. Lin, J. Appl. Phys. **111**, 07C101 (2012).
[6]S. Iihama, Q. Ma, T. Kubota, S. Mizukami, Y. Ando, and T. Miyazaki, Appl. Phys. Express **5**, 083001 (2012).
[7]G. Malinowski, K. C. Kuiper, R. Lavrijsen, H. J. M. Swagten, and B. Koopmans, Appl. Phys. Lett. **94**, 102501 (2009).
[8]C. Bilzer, T. Devolder, J.-V. Kim, G. Counil, C. Chappert, S. Cardoso, and P. P. Freitas, J. Appl. Phys. **100**, 053903 (2006).
[9]A. T. G. Pym, A. Lamperti, B. K. Tanner, T. Dimopoulos, M. Rührig, and J. Wecker, Appl. Phys. Lett. **88**, 162505 (2006).
[10]C. Bilzer, T. Devolder, P. Crozat, and C. Chappert, IEEE Trans. Magn. **44**, 3265 (2008).
[11]R. D. McMichael, M. D. Stiles, P. J. Chen, and J. W. F. Egelhoff, J. Appl. Phys. **83**, 7037 (1998).
[12]G. G. Scott and H. W. Sturner, Phys. Rev. **184**, 490 (1969).
[13]F. Schreiber, J. Pflaum, Z. Frait, T. Mhge, and J. Pelzl, Solid State Commun. **93**, 965 (1995).
[14]E. Francisco and L. Pueyo, Phys. Rev. A **36**, 1978 (1987).
[15]B. Heinrich, J. F. Cochran, M. Kowalewski, J. Kirschner, Z. Celinski, A. S. Arrott, and K. Myrtle, Phys. Rev. B **44**, 9348 (1991).
[16]P. Bruno, Phys. Rev. B **39**, 865 (1989).
[17]V. Kambersky, Czech. J. Phys., Sect. B **26**, 1366 (1976).
[18]A. Lamperti, S.-M. Ahn, B. Ocker, R. Mantovan, and D. Ravelosona, "Interface width evaluation in thin layered CoFeB/MgO superlattices including Ru or Ta buffer layer by X-ray reflectivity," Thin Solid Films (in press).
[19]C. Scheck, L. Cheng, I. Barsukov, Z. Frait, and W. E. Bailey, Phys. Rev. Lett. **98**, 117601 (2007).
[20]Y. Lamy and B. Viala, J. Appl. Phys. **97**, 10F910 (2005).
[21]W. Haiss and J. K. Sass, J. Electroanal. Chem. **386**, 267 (1995).